PHYSICAL REVIEW D **91,** 076012 (2015)

Analytic continuation of the Pasquier inversion representation of the Khuri-Treiman equation

Peng Guo[1,2,*]

[1]*Physics Department, Indiana University, Bloomington, Indiana 47405, USA*
[2]*Center For Exploration of Energy and Matter, Indiana University, Bloomington, Indiana 47408, USA*
(Received 13 January 2015; published 27 April 2015)

The single integral form of the Pasquier inversion representation of the Khuri–Treiman equation presents great advantages for describing the final-state interaction of three-body decay or production processes. However, the original form of the Pasquier inversion representation is only given in the decay region and regions below. For the regions above, analytic continuation of original form is required. Because of the nontrivial nature of the analytic continuation procedure, it is the purpose of this work to obtain a well-defined Pasquier inversion representation of the Khuri–Treiman equation for the entire energy range.

DOI: 10.1103/PhysRevD.91.076012 PACS numbers: 11.55.Fv, 11.80.Et, 13.25.−k

I. INTRODUCTION

The theoretical framework for describing low-energy hadronic three-body interaction has attracted significant attention in the past, and different approaches have been developed, such as field theory based Faddeev- and Bethe–Salpeter-type equations [1–5] and the dispersion relation oriented Khuri–Treiman (KT) equation [6,7]. In processes such as $\eta \to 3\pi$, three-body final-state interaction has been reported to play an important role in explaining the discrepancy of Dalitz plot expansion parameters between experimental measurements and theoretical calculations [8–17].

Among different methods, the dispersion approach based KT equation shows some advantages because of its simplicity of formalism and analog to the naive isobar model approximation [18,19]. Since being first proposed in Ref. [6], the KT equation has been further developed by many authors [7,20–25]. Because of the fact that the KT equation framework is based on the elastic approximation in each subenergy channel, it is often suggested [7,20–24] that the KT equation is suitable for low-energy three-body decay or production processes, such as $\eta/\omega/\phi \to 3\pi$ [9,10,13,14,17,26–31]. The original form of the KT equation is written in a form of a double-integral dispersion equation, one integral coming from the dispersion integration and another relating to partial wave projection. By using the Pasquier inversion technique [23,25,32], the orders of two integrals are being exchanged, and it results in a single integral representation of the KT equation that is more suitable for numerical computation [20–25]. Compared to the double-integral representation of the KT equation that has been used in analyzing processes of $\eta/\omega/\phi \to 3\pi$ in Refs. [9,10,13,14,17,26–31], the Pasquier inversion representation bears great computational advantage since it is a single-integral equation and is entirely defined on the real axis [25]. Therefore, the Pasquier inversion representation is certainly more robust, especially for the purpose of future high-statistics data analysis. Unfortunately, the original form of the Pasquier inversion representation of the KT equation is not well defined for the entire energy range; in fact, the original form is only given in the physical decay region and regions below. For other energy regions, analytic continuation of the Pasquier inversion representation of the KT equation has to be carried out deliberately to avoid singularities generated by contour integrations. As will be discussed in this work, the energy range above the two-particle threshold is divided by a complex contour into three parts: decay, unphysical, and scattering regions. The unphysical region is disconnected from decay and scattering regions; in this region, the original form of the KT equation has to be modified, and an extra term is needed to keep the solution of the KT equation staying on physical sheet. Mathematically, it is certainly interesting to have the Pasquier inversion representation of the KT equation well defined and constructed not just in the physical region but also in the unphysical region. Most importantly, even for some physical purpose, we may still require the amplitude in the unphysical region as well. For example, to extract the light-quark mass difference from $\eta \to 3\pi$, the decay amplitude has to be matched to the χPT prediction [14]. For the sake of convergence of the χPT result, one may choose to match the decay amplitude $T(s,t,u)$ along the line $s = u$, and the matching point is usually chosen for $s = u$ below the two-body threshold, near the Adler zero, for instance [14], such that t usually ends up in the unphysical region above the decay region due to kinematic constraints: $t = M_\eta^2 + 3m_\pi^2 - 2s$. A well-defined solution of the KT equation is thus necessary for such a matching procedure. Because of the nontrivial procedure of analytic continuation, we describe some details of analytic continuation in this work and present a well-defined form of the Pasquier inversion representation of the KT equation in all energy regions.

*pguo@jlab.org

The paper is organized as follows. The original form of the Pasquier inversion representation of the KT equation is briefly introduced in Sec. II. The procedure of analytic continuation is described in Sec. III. The summary and conclusion are given in Sec. IV.

II. SUBENERGY DISPERSION APPROACH TO THREE-BODY FINAL STATE INTERACTION

A general amplitude for a particle with spin-J decaying into three spinless particles, such as in J/ψ decays [33,34], reads

$$\langle 123, \text{out}|J(\lambda), \text{in}\rangle = i(2\pi)^4\delta^4\left(\sum_{i=1,2,3} p_i - P\right)T_\lambda, \quad (1)$$

where we denote the 4-momenta by p_i, P for the ith final-state particle and initial decay particle and λ is the spin projection of the initial state along a fixed axis. Suppressing the isospin coupling among initial and final states, the isobar model amplitude T_λ is given by

$$T_\lambda(s,t,u) = \sum_{S,L,\mu} N_{SL\mu} D^{J*}_{\lambda,\mu}(r_s) d^S_{\mu,0}(\theta_s) a^{(s)}_{SL}(s) + (s \to t) + (s \to u), \quad (2)$$

where the invariants are defined by $s = (p_1 + p_2)^2$, $t = (p_2 + p_3)^2$, and $u = (p_3 + p_1)^2$ and they are constrained by relation $s + t + u = M^2 + \sum_i m_i^2$ (m_i's are final-state particle masses, and M is the mass of the initial particle), $N_{SL\mu} = \sqrt{(2S+1)(2L+1)}\langle S\mu; L0|J\mu\rangle$, and D and d's are the standard Wigner D and d matrices. The spin of pair (12) is denoted by S, and the relative orbital angular momentum between (12) and the third particle is given by L. θ_s is polar angle of particle 1 in the pair (12) rest frame. The rotation r_s, which is given by three Euler angles [33,34], rotates the standard configuration in the (12)3 coupling scheme to the actual one. In the standard configuration of (12)3 coupling (the rest frame of the 3-particle), the third particle moves along the negative z axis while particles 1 and 2 move in the xz plane. The amplitudes in (23)1 and (31)2 coupling schemes (denoted by t and u channel, respectively) are defined in a similar way as in (12)3 coupling (denoted by s channel). The dynamics of the decay process is described by scalar functions $a^{(s,t,u)}_{SL}$, which only depend on the subenergy of isobar pairs and possess only a unitarity cut in subenergy by assumption [21–23].

For simplicity, in the following discussion, we consider the decay of a scalar particle, $J = 0$, and truncate the partial waves to include only the S wave: $S = L = 0$. Masses of final particles are assumed identical, $m_1 = m_2 = m_3 = m$, and subchannels are assumed symmetric: $a^{(s)}_{00} = a^{(t)}_{00} = a^{(u)}_{00} = a$. Thus, the decay amplitude is simply given by sum of three terms,

$$T(s,t,u) = a(s) + a(t) + a(u). \quad (3)$$

A. Khuri–Treiman equation and Pasquier inversion representation

The discontinuity of the decay amplitude crossing the unitarity cut in a subenergy, such as s, is given by

$$\triangle T(s,t,u) = \frac{T(s+i\epsilon,t,u) - T(s-i\epsilon,t,u)}{2i} = \rho(s) f^*(s)\frac{1}{2}\int_{-1}^{1} dz_s T(s,t,u), \quad (4)$$

where $\rho(s) = \sqrt{1-4m^2/s}$ and $f(s)$ denotes an S-wave two-body elastic scattering amplitude and is parametrized by a phase shift of two-body scattering, $f = (e^{2i\delta}-1)/2i\rho$. $z_s = \cos\theta_s$ is given by $z_s = -(t-u)/\rho(s)k(s)$, where $k(s) = \sqrt{[s-(M-m)^2][s-(M+m)^2]}$. A diagrammatic representation of discontinuity relations in Eq. (4) is shown in Fig. 1.

By assumption, a's possess only unitarity cuts; thus, $\Delta T(s,t,u) = \Delta a(s)$, and

$$\Delta a(s) = \rho(s) f^*(s)\left[a(s) + \frac{2}{\rho(s)k(s)}\int_{t_-(s)}^{t_+(s)} (\Gamma) dt a(t)\right], \quad (5)$$

where the factor 2 in front of contour integral takes into account the contribution for the u channel. As discussed in Refs. [21–23,25], the angular projection in Eq. (4) is replaced by a contour integration in the complex plane according to perturbation theory [7,35]; contour Γ is given in Fig. 2. The boundaries of the Dalitz plot, $t_\pm(s)$, are given by the solutions of $\phi(s,t_\pm) = 0$, where $\phi(s,t) = stu - m^2(M^2-m^2)^2$, and the analytic continuation of $t_\pm(s)$ in s is specified by Γ; see Fig. 2. The scalar function a then is determined by the subenergy dispersion relation,

$$a(s) = \frac{1}{\pi}\int_{4m^2}^{\infty} ds' \frac{1}{s'-s}\Delta a(s'). \quad (6)$$

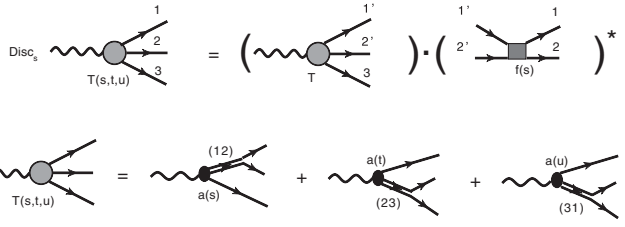

FIG. 1. A diagrammatic representation of discontinuity relations in Eq. (4).

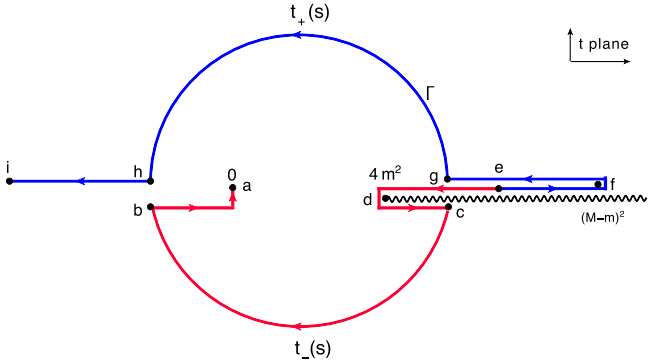

FIG. 2 (color online). The path of $t_{\pm}(s)$ in the t complex plane as s increased from $4m^2$ to ∞. The black wiggly line represents right-hand cuts of the $g(t)$ function. The points labeled by $a-i$ correspond to a) $t_{-}(\infty)=0$, b) $t_{-}((M+m)^2)=m(m-M)$, c) $t_{-}((M-m)^2)=m(M+m)$, d) $t_{-}((M^2-m^2)/2)=4m^2$, e) $t_{\pm}(4m^2)=(M^2-m^2)/2$, f) $t_{+}(m(M+m))=(M-m)^2$, g) $t_{+}((M-m)^2)=m(M+m)$, h) $t_{+}((M+m)^2)=m(m-M)$, and i) $t_{+}(\infty)=-\infty$, respectively.

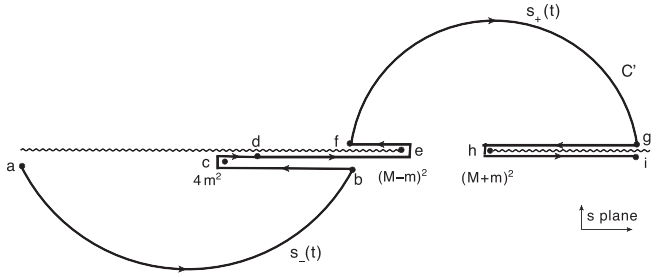

FIG. 3. The path of $s_{\pm}(t)$ in the s complex plane for $t\in[-\infty,(M-m)^2]$. The arrows indicate the directions that invariants follow along the path of integrations. The black wiggly lines represent cuts attached to two branch points: $(M\pm m)^2$ in the s plane. The points labeled by $a-i$ correspond to a) $s_{-}(0)=-\infty$, b) $s_{-}(4m^2)=(M^2-m^2)/2$, c) $s_{-}((M^2-m^2)/2)=4m^2$, d) $s_{\pm}((M-m)^2)=m(m+M)$, e) $s_{+}(m(M+m))=(M-m)^2$, f) $s_{+}(4m^2)=(M^2-m^2)/2$, g) $s_{+}(0)=\infty$, h) $s_{+}(m(m-M))=(M+m)^2$, and i) $s_{+}(-\infty)=\infty$, respectively.

As discussed in Ref. [25], usually, it is useful to parametrize a as a product of a known function and a reduced amplitude. For instance, we may choose parametrization, $a(s)=f(s)g(s)$, and thus the discontinuity relation for the reduced amplitude g is given by [25]

$$\Delta g(s)=-\theta(s_L-s)\frac{\mathrm{Im}f(s)}{f^*(s)}g(s)+\theta(s-4m^2)\frac{2}{k(s)}\int_{t_+(s)}^{t_-(s)}(\Gamma)dtf(t)g(t), \tag{7}$$

where s_L labels the branch point of the left-hand cut in $f(s)$, and

$$g(s)=\frac{1}{\pi}\int_{-\infty}^{\infty}ds'\frac{1}{s'-s}\Delta g(s'). \tag{8}$$

By using the Pasquier inversion technique [21–23,25], also see Appendix A, we may obtain a single integral equation for g,

$$g(s)=-\frac{1}{\pi}\int_{-\infty}^{s_L}ds'\frac{1}{s'-s}\frac{\mathrm{Im}f(s')}{f^*(s')}g(s')+g_R(s), \tag{9}$$

where

$$g_R(s)=\frac{2}{\pi}\int_{-\infty}^{(M-m)^2}dtf(t)g(t)[\theta(t)\Delta(s,t)-\theta(-t)\Sigma(s,t)]. \tag{10}$$

The kernel functions Δ and Σ are given by

$$\Delta(s,t)=\int_{s_-(t)}^{s_+(t)}(C')ds'\frac{1}{U(s')}\frac{1}{s'-s}, \tag{11}$$

$$\Sigma(s,t)=\int_{s_+(t)}^{s_+(\infty)}(C')ds'\frac{1}{U(s')}\frac{1}{s'-s}, \tag{12}$$

where the square-root function $U(s)=\sqrt{[s-(M-m)^2][s-(M+m)^2]}$ is defined in the complex-s plane and the phase convention for $U(s)$ is chosen by $U(s\pm i0)=(\mp,i,\pm)|U(s)|$ for $s\in([-\infty,(M-m)^2],[(M-m)^2,(M+m)^2],[(M+m)^2,\infty])$. respectively. Thus, the square root $k(s)$ is given by the value of $U(s)$ right below two cuts attached to $(M\pm m)^2$, $k(s)=U(s-i0)$. The contour C' is given in Fig. 3, and $s_{\pm}(t)$ are specified by solutions of $\phi(s_{\pm},t)=0$ and contour C'.

The Pasquier inversion representation of $g(s)$ in Eqs. (9) and (10) is initially defined in the range $s\in[-\infty,(M-m)^2]$ (on the left and upper sides of contour C'). As will be made clear in Sec. III, contour C' in kernel functions, Δ and Σ, is singular and divides the s plane into several isolated regions. Therefore, Eqs. (9) and (10) can only hold for a complex s that stays at the same side of contour C' and does not cross contour C'. When s is taken to cross contour C' to reach the region on the other side, for the Pasquier inversion representation of the KT equation to stay on the physical sheet, C' has to be deformed, and an extra piece is picked up as the consequence of the deformation of the contour. In what follows, we present the procedure of analytic continuation of the Pasquier inversion representation of the KT equation into $s\in[(M-m)^2,\infty]$ regions.

III. ANALYTIC CONTINUATION OF PASQUIER INVERSION REPRESENTATION FOR $S \in [(M-m)^2,\infty]$

As mentioned previously, $g(s)$ given by Eqs. (9) and (10) is originally defined for $s \in [-\infty,(M-m)^2]$. The analytic continuation of first term on right-hand side of Eq. (9) shows no difficulty, and therefore we will only focus on the second term on the right-hand side of Eq. (9), $g_R(s)$, in following discussion. The s dependence of $g(s)$ on the second term, $g_R(s)$, is through kernel functions Δ and Σ, and Δ and Σ on physical sheet for $s \in [-\infty,(M-m)^2]$ are given by the value of s running along the black wiggly line attached to $(M-m)^2$ in Fig. 3. Therefore, the strategy of analytic continuation is that we start from here and then increase s continuously until a singularity is encountered. Unfortunately for $g_R(s)$, contour C' presents a cut in the complex-s plane, which stops us from naively using Eqs. (9) and (10) in the nearby region $s \in [(M-m)^2, (M+m)^2]$. To illustrate this point, we first use the technique presented in Appendix A and rewrite $g_R(s)$ as

$$g_R(s) = \frac{2}{\pi}\int_{\Gamma'} dta(t) \int_{s_{\Gamma'}(t)}^{\infty} (C')ds' \frac{1}{s'-s}\frac{1}{U(s')}, \qquad (13)$$

where contour Γ' is given in Fig. 7 and the location of $s_{\Gamma'}(t)$ on C' is specified by the location of t on Γ'; see more details in Appendix A. Exchanging the order of two integrals leads to

$$g_R(s) = \frac{2}{\pi}\int_{C'} ds' \frac{1}{s'-s}\frac{1}{U(s')}\int_0^{t_{C'}(s')} (\Gamma')dta(t), \qquad (14)$$

where $t_{C'}(s')$ is the inverse of $s_{\Gamma'}(t)$ and Eq. (14) is similar to Eq. (A3) but with contours C' and Γ' instead. Now, we can clearly see the cut structure on s generated by contour C' in Eq. (14). As s is moved from the left-hand side of C' in the region $s \in [-\infty,(M-m)^2]$ to reach the $s \in [(M-m)^2,(M+m)^2]$ region by crossing contour C' (the motion of s is demonstrated in Fig. 4 by a red dashed curve), C' has to be deformed to keep $g_R(s)$ on the physical sheet. For example, at a point, s_A, in Fig. 4, which sits right next to the inside circle of C' in the complex plane, $g_R(s_A)$ on the physical sheet is given by

$$g_R(s_A) = \frac{2}{\pi}\int_{C'} ds' \frac{1}{s'-s_A}\frac{1}{U(s')}\int_0^{t_{C'}(s')} (\Gamma')dta(t) + \frac{4i}{U(s_A)}\int_0^{t_{C'}(s_A)} (\Gamma')dta(t). \qquad (15)$$

Next, s is moved away from s_A to a point on the real axis in region $s \in [(M-m)^2,(M+m)^2]$, such as s_B in Fig. 4, and thus C' is further deformed to follow the motion of s. When s reaches the real axis, C' in the second term on the right-hand side of Eq. (15) collapses onto the real axis, and Γ' opens up accordingly into Γ; thus, for $s \in [(M-m)^2, (M+m)^2]$ on the real axis, we obtain

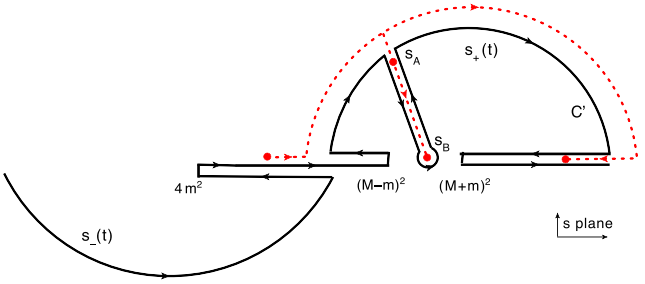

FIG. 4 (color online). Analytic continuation of a function of type $g_R(s)$ in Eq. (14) is followed by the motion of s (red dashed curve). The physical sheet of $g_R(s)$ is defined in the upper half-plane that is divided by contour C'. The lower half-plane can be reached by crossing C', and when it does, a discontinuity has to be picked up to keep $g_R(s)$ on the physical sheet.

$$g_R(s) = \frac{2}{\pi}\int_{-\infty}^{(M-m)^2} dta(t)[\theta(t)\Delta(s,t) - \theta(-t)\Sigma(s,t)] + \frac{4i}{U(s)}\int_0^{t_+(s)} (\Gamma)dta(t), \quad \text{for } s \in [(M-m)^2, \quad (M+m)^2]. \qquad (16)$$

At last, the analytic continuation of $g_R(s)$ from $s \in [-\infty,(M-m)^2]$ to region $s \in [(M+m)^2,\infty]$, where s runs along the black wiggly line attached to $(M+m)^2$ in Fig. 3, does not encounter any singularities, and so it does not require the deformation of contour C'—see the motion of the red dashed curve in Fig. 4—and therefore $g_R(s)$ in Eq. (10) remains unchanged for $s \in [(M+m)^2,\infty]$.

On the other hand, we may also perform the analytic continuation of the Pasquier inversion representation of the KT equation through a triangle diagram. Using Eq. (6), we first rewrite Eqs. (9) and (10) as

$$g(s) = -\frac{1}{\pi}\int_{-\infty}^{s_L} ds' \frac{1}{s'-s}\frac{\mathrm{Im}f(s')}{f^*(s')}g(s') + \frac{2}{\pi}\int_{4m^2}^{\infty} dt' \Delta a(t')\mathcal{G}(s,t'), \quad \text{for } s < (M-m)^2, \qquad (17)$$

where $\mathcal{G}$ is given by

$$\mathcal{G}(s,t') = \frac{1}{\pi}\int_{-\infty}^{(M-m)^2} dt \frac{1}{t'-t}[\theta(t)\Delta(s,t) - \theta(-t)\Sigma(s,t)], \quad \text{for } t' > 4m^2, \quad s < (M-m)^2. \qquad (18)$$

$\mathcal{G}$ is identified as the Pasquier inversion representation of a triangle diagram in the region $t' > 4m^2, s < (M-m)^2$.

The analytic continuation of $\mathcal{G}$ in different representations is presented in Appendix B, and the Pasquier inversion representation of $\mathcal{G}$ for $(s,t') \in [-\infty,\infty]$ is given by Eq. (B11),

$$\mathcal{G}(s,t') = \frac{1}{\pi}\int_{-\infty}^{(M-m)^2} dt \frac{1}{t'-t}[\theta(t)\Delta(s,t) - \theta(-t)\Sigma(s,t)] + 2i\theta(s-(M-m)^2)\theta((M+m)^2-s) \times \left[\frac{1}{U(s)}\int_0^{t_+(s)}(\Gamma)\frac{dt}{t'-t} + \theta(t')\theta(4m^2-t')\frac{2\pi i}{U(s)}\right], \quad \text{for } (s,t') \in [-\infty,\infty].$$

The s dependence of $g(s)$ in the second term in Eq. (17) is all through triangle diagram $\mathcal{G}$; thus, the analytic continuation of $\mathcal{G}$ completes the analytic continuation of the Pasquier inversion representation of $g(s)$. Plugging Eq. (B11) back into Eq. (17), we once again obtain the Pasquier inversion representation of $g(s)$ for $s \in [-\infty,\infty]$,

$$g(s) = -\frac{1}{\pi}\int_{-\infty}^{s_L} ds' \frac{1}{s'-s}\frac{\mathrm{Im}f(s')}{f^*(s')}g(s') + \frac{2}{\pi}\int_{-\infty}^{(M-m)^2} dt f(t)g(t)[\theta(t)\Delta(s,t) - \theta(-t)\Sigma(s,t)] + 4i\theta(s-(M-m)^2)\theta((M+m)^2-s) \times \frac{1}{U(s)}\int_0^{t_+(s)}(\Gamma)dtf(t)g(t), \quad \text{for } s \in [-\infty,\infty]. \tag{19}$$

The analytic continuation of the Pasquier inversion representation of $g(s)$ given by Eq. (19) is tested numerically by using a toy model for $f(s)$, and the model of $f(s)$ is taken from Ref. [25]. The comparison of $g(s)$'s by solving the Pasquier inversion representation Eq. (19) and the dispersion representation Eqs. (7) and (8) is shown in Fig. 5. We also show the results by solving Eqs. (9) and (10) without proper analytic continuation compared to the contribution of the extra term that is picked up by analytic continuation, $4i/U(s)\int_0^{t_+(s)}(\Gamma)dta(t)$. As demonstrated in Fig. 5, the solution of analytic continuation of the Pasquier inversion representation of $g(s)$ is consistent with the dispersion representation of $g(s)$. Without the proper analytic continuation, the solution of Pasquier inversion representation of $g(s)$ jumps in unphysical region $s \in [(M-m)^2,(M+m)^2]$. In order to keep $g(s)$ continuous and staying on physical sheet, an extra term, $4i/U(s)\int_0^{t_+(s)}(\Gamma)dta(t)$, is required.

At last, similarly, if we parametrize $a(s) = G(s)/D(s)$ [25], where $D(s) = N(s)/f(s)$ contains only the unitarity cut of the scattering amplitude and all other cuts are absorbed into function $N(s)$ [36,37], we thus obtain

$$G(s) = \frac{2}{\pi}\int_{-\infty}^{(M-m)^2} dt \frac{G(t)}{D(t)}[\theta(t)\Delta_G(s,t) - \theta(-t)\Sigma_G(s,t)] + 4i\theta(s-(M-m)^2)\theta((M+m)^2-s) \times \frac{N(s)}{U(s)}\int_0^{t_+(s)}(\Gamma)dt\frac{G(t)}{D(t)}, \quad \text{for } s \in [-\infty,\infty], \tag{20}$$

where the kernel functions Δ_G and Σ_G are given by Eqs. (A9) and (A10), respectively.

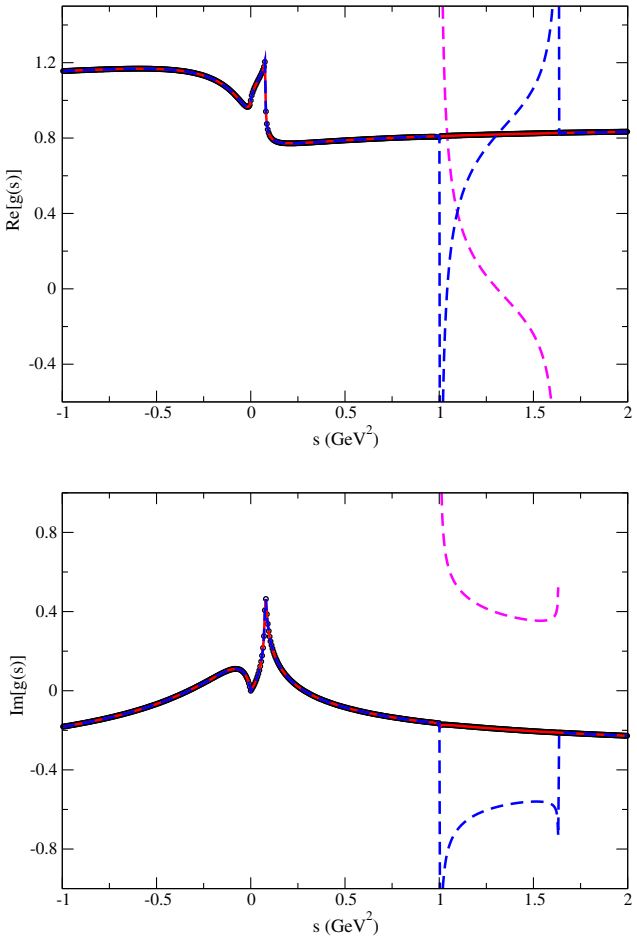

FIG. 5 (color online). The real (top plot) and imaginary (bottom plot) parts of $g(s)$ by solving both the dispersion representation Eqs. (7) and (8) (black circles) and Pasquier inversion representation Eq. (19) (solid red curves). Blue dashed curves are the solution of $g(s)$ from Eqs. (9) and (10) without proper analytic continuation, and purple dashed curves represent the contribution from the extra term picked up by analytic continuation in Eq. (19), $4i/U(s)\int_0^{t_+(s)}(\Gamma)dta(t)$. The input model of $f(s)$ is taken from Eq. (28) in Ref. [25], with fixed parameters: $\alpha = 0.1$, $\beta = 0.2$, $m_R = 0.8$ GeV, $m = 0.14$ GeV, and $M = 1.14$ GeV. The left-hand cut of $f(s)$ is placed at $s_L = 0$, and $g(s)$ is normalized to $g(0) = 1$.

IV. SUMMARY

We presented the analytic continuation procedure of the Pasquier inversion representation of the KT equation, and a well-defined Pasquier inversion representation of the KT equation for an arbitrary s on the real axis is given by Eqs. (19) and (20).

Comparing the Pasquier inversion representation of the KT equation in Eq. (19) to the dispersion representation of the KT equation in Eqs. (7) and (8), as has been also discussed in Ref. [25], the single integral form of the Pasquier inversion representation in Eq. (19) indeed presents a significant advantage in numerical computation in regions $s \in [-\infty, (M-m)^2]$ and $s \in [(M-m)^2, \infty]$. However, in the unphysical region $s \in [(M-m)^2, (M+m)^2]$, the dispersion representation in Eqs. (7) and (8) requires no extra effort, but analytic continuation of the Pasquier inversion representation becomes nontrivial and needs an extra term to keep solution $g(s)$ staying on the physical sheet. At last, we solved the Pasquier inversion representation of the KT equation in Eq. (19) numerically by using a toy model of $f(s)$, and solutions with and without proper analytic continuation compared to the solution of the dispersion representation are illustrated in Fig. 5.

ACKNOWLEDGMENTS

We thank Adam P. Szczepaniak for many fruitful discussions. We acknowledge support in part by the U.S. Department of Energy under Grant No. DE-FG0287ER40365 and the Indiana University Collaborative Research Grant and U.S. National Science Foundation under Grant No. PHY-1205019. We also acknowledge support from the U.S. Department of Energy Contract No. DE-AC05-06OR23177, under which Jefferson Science Associates, LLC, manages and operates Jefferson Laboratory.

APPENDIX A: PASQUIER INVERSION TECHNIQUE

For completeness, we present the Pasquier inversion technique [23,32] in this section. Considering a double-integral equation of the type

$$I(s) = \int_{4m^2}^{\infty} ds' \frac{1}{s'-s} \frac{N(s')}{k(s')} \int_{t_-(s')}^{t_+(s')} (\Gamma) dt a(t), \qquad \text{(A1)}$$

where contour Γ followed by t integration is defined to avoid a unitarity cut in a, see Fig. 2, and the integration path of s' is defined on the real axis, the physical value of $I(s)$ is given by s running above the real axis.

As described in Refs. [23,32], we first split the t integral into two pieces and rewrite the double integrals in Eq. (A1) as

$$I(s) = \int_{4m^2}^{\infty} ds' \frac{1}{s'-s} \frac{N(s')}{k(s')} \left[\int_0^{t_+(s')} (\Gamma) - \int_0^{t_-(s')} (\Gamma) \right] dt a(t). \qquad \text{(A2)}$$

Then, for first term in brackets in Eq. (A2), the path of s' integration is shifted to above the real axis, and for the second term in brackets in Eq. (A2), the path of s' integration is shifted to below the real axis. Note that the kinematic function $k(s')$ as a function of s' has two branch points: $(M \pm m)^2$. Two cuts may be attached to these two points: one runs from $-\infty$ up to $(M-m)^2$, and another runs from $(M+m)^2$ up to ∞; see the black wiggly lines in Fig. 6. As we have mentioned before, U is defined as the continuation of $k(s')$ for a complex argument, and the physical value of $k(s')$ is given by taking the branch of $U(s')$ below two cuts attached to $(M \pm m)^2$, $k(s') = U(s' - i0)$. These two kinematic cuts are placed above both the real axis and shifted s' integration paths described previously (see Fig. 6); therefore, the operation of shifting s' integration paths is valid, and s' integration paths do not interfere with cuts in U. Thus, we can safely rewrite the double integrals in Eq. (A2) as

$$I(s) = \int_C ds' \frac{1}{s'-s} \frac{N(s')}{U(s')} \int_0^{t_C(s')} (\Gamma) dt a(t), \qquad \text{(A3)}$$

where the path C of the s' integral is shown in Fig. 6, and whether $t_C(s')$ is $t_+(s')$ or $t_-(s')$ depends on which portion of path C the invariant s' is on. $t_+(t_-)$ is assigned to s' on the portion of C above (below) the real axis. In Eq. (A3), the physical value of $I(s)$ is given by s running above contour C. Next, we exchange the order of two integrals so that Eq. (A3) becomes

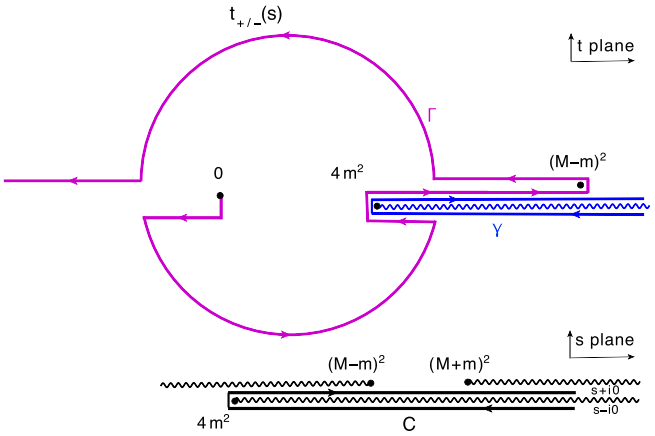

FIG. 6 (color online). The path of $t_\pm(s)$ (solid purple curves), contour C (solid black lines), and γ (solid blue lines). The arrows indicate the directions that invariants follow in double integrations, Eqs. (A1) and (A4). The blue wiggly line represents the unitarity cut in the t plane, and the black wiggly lines represent the cuts in the s plane.

$$I(s) = \int_\Gamma dt a(t) \left[\int_{s_\Gamma(t)}^{\infty} (C) ds' \frac{1}{s'-s} \frac{N(s')}{U(s')} \right], \quad \text{(A4)}$$

where t integration on contour Γ runs from 0 to $-\infty$ by looping around threshold $(M-m)^2$, see Fig. 6, and s' integration runs from $s_\Gamma(t)$ up to ∞ along path C, and $s_\Gamma(t)$ is given by the inverse of $t_C(s')$. By assumption, a has only the unitarity cut, and using Cauchy's theorem, we can write an equation,

$$a(t) = \frac{1}{2\pi i} \int_\gamma dt' \frac{a(t')}{t'-t}, \quad \text{(A5)}$$

where contour γ loops around the unitarity cut but avoids interference with Γ, see in Fig. 6, and the convergence of integration has been assumed valid so that the circle of contour γ at infinity can be dropped. Thus, we obtain

$$I(s) = \frac{1}{2\pi i} \int_\gamma dt' a(t') \left[\int_\Gamma \frac{dt}{t'-t} \int_{s_\Gamma(t)}^{\infty} (C) ds' \frac{1}{s'-s} \frac{N(s')}{U(s')} \right]. \quad \text{(A6)}$$

When the N function is replaced by a constant, the function in brackets in Eq. (A6) may be associated to a triangle diagram; see Appendix B. The next step is to deform the contour γ onto the real axis toward $-\infty$ but avoid both the unitarity cut in a and the singularities from the expression in brackets in Eq. (A6). By construction of Γ, the unitarity cut of a sits along the blue wiggly line in Fig. 6, and $a(t)$ for t running above the unitarity cut is defined as physical. Therefore, as long as the deformation of γ and Γ toward the negative real axis does not interfere with the unitarity cut of a, a remains on the physical sheet all the time. Singularities of the function in brackets in Eq. (A6) have been extensively studied by authors in Refs. [21,23,38–40] from a perturbation theory perspective, and they are branch points at $t = 0, 4m^2$ and $(M-m)^2$. One may attach branch cuts to those branch points running toward the negative real axis [21,23,38–40]; therefore, the contour γ' may be chosen to loop around the threshold $(M-m)^2$ toward the negative real axis. The deformation of contour γ also drags the contour Γ going with it back onto the real axis, and the correspondent contour C must then be opened up accordingly. Simultaneously, for $I(s)$ staying on physical sheet, some s are also dragged by the deformation of C into the complex plane, and the physical value of $I(s)$ is now given by an s that sits on the same side of C when it opens up into the complex plane. The only t'-dependent singularities come from factor $1/(t'-t)$ in brackets in Eq. (A6) so that, when contour γ is collapsed onto the real axis, the discontinuity of this factor $1/(t'-t)$ along the cut from $-\infty$ to $(M-m)^2$ is picked up. Equivalently, we may replace $\int_\gamma dt'/(t'-t)$ by $2\pi i \int_{-\infty}^{(M-m)^2} dt' \delta(t'-t)$ in Eq. (A6). Therefore, Eq. (A6) becomes

$$I(s) = \int_{\Gamma'} dt a(t) \left[\int_{s_{\Gamma'}(t)}^{\infty} (C') ds' \frac{1}{s'-s} \frac{N(s')}{U(s')} \right]. \quad \text{(A7)}$$

The contours C' and Γ' have to be chosen to avoid the singularities in integrands. Examining Eq. (A7), we note that integrands of contour integration over invariant s' are only the product of $1/(s'-s)$, the kinematic function U, and the left-hand cut function N. As we mentioned earlier, the kinematic function U as a function of s' has two branch points, $(M \pm m)^2$; two cuts are attached to these two points with one running toward $-\infty$ and another running toward ∞; see the black wiggly lines in Fig. 7. Therefore, the contour C' may be chosen to avoid two cuts attached to $(M \pm m)^2$, as plotted in Fig. 7. With this choice, the function in brackets in Eq. (A7) may be associated with the discontinuities of the triangle diagram defined in Eq. (A6) along the cut attached to branch point $(M-m)^2$ in the t plane. Similarly to γ', the contour Γ' also loops around the point $(M-m)^2$ and is placed above the unitarity cut in a. Whether $s_{\Gamma'}(t)$ is $s_+(t)$ or $s_-(t)$ depends on whether t is above or below the cut attached to $(M-m)^2$ in the t plane; see Fig. 7.

As mentioned earlier, the physical value of $I(s)$ was chosen by s running above contour C in Eq. (A3), when C is deformed to C'; see Figs. 6 and 7. For $I(s)$ to stay on the physical sheet, s is not allowed to cross the contour, and as a result, some s are forced to follow the deformation of the contour into the complex plane. Specifically, 1) for $s \in [-\infty, (M-m)^2]$, the physical value of $I(s)$ is given by s running along the black wiggly line attached to $(M-m)^2$; 2) for $s \in [(M-m)^2, \infty]$, now physical $I(s)$ is trapped into the value of s running along the black wiggly line attached to $(M+m)^2$ between sections $g-h$ and $h-i$ on C'; and 3) the form of $I(s)$ in Eq. (A7) for $s \in [(M-m)^2, (M+m)^2]$ on the real axis is no longer on the physical sheet, and physical $I(s)$ now is given by a complex s running on the upper side of the arc $f-g$ on C'.

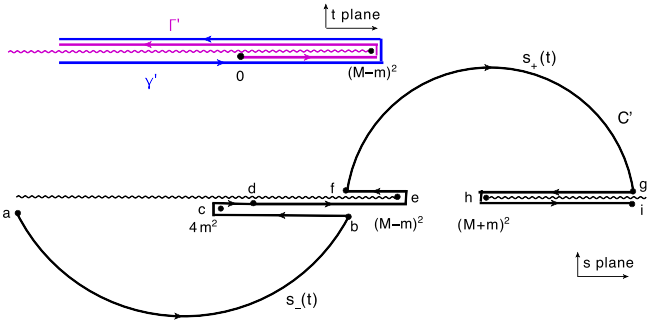

FIG. 7 (color online). The contour Γ' (solid purple lines), C' (solid black curves), and γ' (solid blue lines) in Eq. (A7). The arrows indicate the directions that invariants follow along the path of integrations. The purple and black wiggly lines represent the unitarity cut in the s plane and cuts attached to two branch points, $(M \pm m)^2$, in the s plane, respectively.

To reach physical $I(s)$ for $s \in [(M-m)^2, (M+m)^2]$ on the real axis, the analytic continuation is required, and the procedure is described in Sec. III.

At last, by splitting the s' integration path, $\int_{\Gamma'} = [\int_{0_-}^{(M-m)^2_-} - \int_{0_+}^{(M-m)^2_+}] + \int_{0_+}^{-\infty_+}$, in Eq. (A7) [subscript $+/-$ of the integration limits denotes the path of integration lying above or below the cut attached to branch point $(M-m)^2$ in the t plane; see Fig. 7], we obtain

$$I(s) = \int_{-\infty}^{(M-m)^2} dt a(t)[\theta(t)\Delta_G(s,t) - \theta(-t)\Sigma_G(s,t)], \tag{A8}$$

where

$$\Delta_G(s,t) = \int_{s_-(t)}^{s_+(t)} (C') ds' \frac{1}{s'-s}\frac{N(s')}{U(s')}, \tag{A9}$$

$$\Sigma_G(s,t) = \int_{s_+(t)}^{\infty} (C') ds' \frac{1}{s'-s}\frac{N(s')}{U(s')}. \tag{A10}$$

For s on the real axis, the value of Δ_G and Σ_G on the physical sheet is only defined in regions $[-\infty, (M-m)^2]$ and $[(M+m)^2, \infty]$. For $s \in [(M-m)^2, (M+m)^2]$, Δ_G and Σ_G given by Eqs. (A9) and (A10) without proper analytic continuation are on the unphysical sheet. For the case $N(s) = 1$, the corresponding kernels are denoted as Δ and Σ.

Kernel functions Δ and Σ can be expressed in terms of elementary functions. For real s and t, the values of Δ and Σ given below by Eqs. (A11)–(A14) are simply corresponding to the limits $s + i0$ and $t + i0$, and again Eqs. (A12) and (A14) are defined on the unphysical sheet,

$$\Delta(s,t) = \frac{1}{U(s)}\ln\left|\frac{R(s,t)+U(s)U(t)}{R(s,t)-U(s)U(t)}\right| - \theta(\phi(s,t))\frac{i\pi}{U(s)},$$
$$\text{for } t \in [0,(M-m)^2], \quad s \in [-\infty,(M-m)^2] \,\&\, [(M+m)^2,\infty], \tag{A11}$$

and

$$\Delta(s,t) = \frac{1}{U(s)}\ln\frac{R(s,t)+U(s)U(t)}{R(s,t)-U(s)U(t)} - \theta(m(m+M)-t)\theta(s_R(t)-s)\frac{2i\pi}{U(s)},$$
$$\text{for } t \in [0,(M-m)^2], \quad s \in [(M-m)^2,(M+m)^2], \tag{A12}$$

where $R(s,t) = -M^4 + (s-m^2)(t-m^2) + M^2(s+t)$ and $s_R(t)$ is given by the solution of $R(s_R,t) = 0$,

$$\Sigma(s,t) = \frac{1}{U(s)}\ln|L(s,t)| - \theta(s-s_+(t))\frac{i\pi}{U(s)},$$
$$\text{for } t < 0, \quad s \in [-\infty,(M-m)^2] \,\&\, [(M+m)^2,\infty], \tag{A13}$$

and

$$\Sigma(s,t) = \frac{1}{U(s)}\ln L(s,t) - \theta(\mathrm{Im}L(s,t))\frac{2i\pi}{U(s)},$$
$$\text{for } t < 0, \quad s \in [(M-m)^2,(M+m)^2], \tag{A14}$$

where

$$L(s,t) = \frac{[s_+(t)-s][s-M^2-m^2+U(s)]}{[s_+(t)-s](s-M^2-m^2)+U^2(s)-U(s)U(s_+(t))}.$$

APPENDIX B: DIFFERENT REPRESENTATIONS OF A TRIANGLE DIAGRAM

From perturbation theory, the Feynman parametrization of the triangle diagram in Fig. 8 is given by Ref. [7],

$$\mathcal{G}(s,t) = \frac{1}{\pi}\int_0^1 d\alpha_1 d\alpha_2 d\alpha_3 \times \frac{\delta(1-\alpha_1-\alpha_2-\alpha_3)}{\alpha_1 t + (1-\alpha_1-\alpha_1\alpha_2)m^2 - \alpha_3(\alpha_1 M^2 + \alpha_2 s) - i\epsilon}, \tag{B1}$$

where t denotes the invariant mass square of the pair (23) propagator. The analytic continuation of the Feynman parametrization representation of $\mathcal{G}$ as a function of complex arguments (s,t) is carried out by the $i\epsilon$ prescription [7].

In what follows, we present the analytic continuation of both the dispersion representation and the Pasquier inversion representation of $\mathcal{G}$; the strategy is that we start at a region in which a representation of $\mathcal{G}$ is defined on the physical sheet and consistent with perturbation theory result Eq. (B1), then, $\mathcal{G}$ is continued to other regions by using the perturbation theory result Eq. (B1) as a reference:

(1) The dispersion representation of a triangle diagram for $t > 4m^2$ has been discussed in Ref. [7],

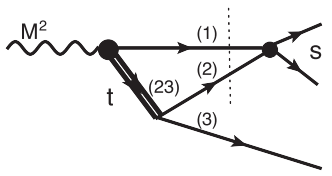

FIG. 8. A triangle diagram with a fixed internal mass $\sqrt{t}$ in the (23) subchannel.

$$\mathcal{G}(s,t)=\frac{1}{\pi}\int_{4m^2}^{\infty}ds'\frac{1}{s'-s}\left[\frac{1}{k(s')}\int_{t_-(s')}^{t_+(s')}(\Gamma)dt'\frac{1}{t-t'}\right],$$
$$\text{for } t>4m^2. \tag{B2}$$

(2) The Pasquier inversion representation of a triangle diagram for $s<(M-m)^2$ is given by Ref. [25],

$$\mathcal{G}(s,t)=\frac{1}{\pi}\int_{-\infty}^{(M-m)^2}\frac{dt'}{t-t'}\times[\theta(t')\Delta(s,t')-\theta(-t')\Sigma(s,t')],$$
$$\text{for } s<(M-m)^2. \tag{B3}$$

1. Analytic continuation of the dispersion representation of the triangle diagram

We first perform analytic continuation of the dispersion representation of $\mathcal{G}$ in Eq. (B2). Note that the overlapping region for both the dispersion representation and the Pasquier inversion representation of $\mathcal{G}$ on the physical sheet is $t\in[4m^2,\infty]$ and $s\in[-\infty,(M-m)^2]$. As described in Appendix A, exchanging the order of double integrals encounters no extra singularities in this region, so we start from here and rewrite Eq. (B2) as, see Eqs. (A1)–(A4),

$$\mathcal{G}(s,t)=\frac{1}{\pi}\int_{\Gamma}dt'\frac{1}{t-t'}\left[\int_{s_\Gamma(t')}^{\infty}(C)ds'\frac{1}{s'-s}\frac{1}{U(s')}\right],$$
$$\text{for } t>4m^2,\qquad s<(M-m)^2. \tag{B4}$$

The cut in t generated by contour Γ is now explicitly given by $\int_\Gamma dt'/(t-t')$; we start with t running along the black wiggly line in Fig. 2, where $\mathcal{G}$ is defined on the physical sheet. As long as the motion of t in the complex plane does not interfere with the contour Γ, $\mathcal{G}$ remains on the physical sheet, and thus Eq. (B2) still holds for $t<0$; see the motion of t represented by the black dashed curve in Fig. 9. However, when t is moved to cross contour Γ, the contour Γ has to be deformed to keep $\mathcal{G}$ on the physical sheet. To reach region $t\in[0,4m^2]$, we can first move t to t_A, which is a point that sits right inside the circle of Γ; see Fig. 9. Thus, the deformation of Γ leads to

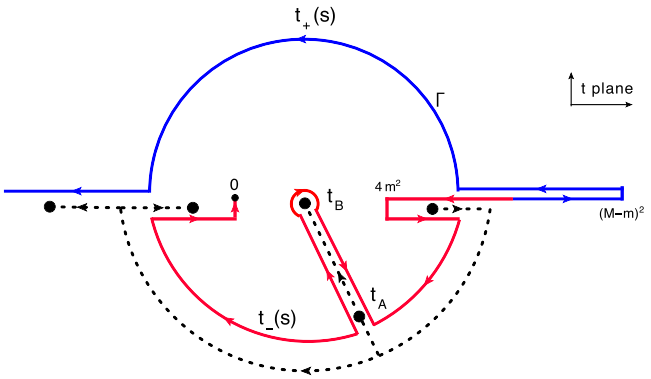

FIG. 9 (color online). Analytic continuation of a function in t of type $\mathcal{G}(s,t)$ in Eq. (B4) is followed by the motion of t (black dashed curve). The physical sheet of $\mathcal{G}(s,t)$ in t is defined in the outside space of Γ. $t\in[0,4m^2]$ inside of the Γ region can be reached by crossing Γ, and then a discontinuity has to be picked up to keep $\mathcal{G}(s,t)$ on the physical sheet.

$$\mathcal{G}(s,t_A)=\frac{1}{\pi}\int_{\Gamma}dt'\frac{1}{t_A-t'}\left[\int_{s_\Gamma(t')}^{\infty}(C)ds'\frac{1}{s'-s}\frac{1}{U(s')}\right]+2i\int_{s_\Gamma(t_A)}^{\infty}(C)ds'\frac{1}{s'-s}\frac{1}{U(s')},$$
$$\text{for } s<(M-m)^2. \tag{B5}$$

When t_A is moved to $t_B\in[0,4m^2]$ on the real axis, contour Γ in the second piece on the right-hand side of Eq. (B5) is dragged by the motion of t to collapse onto the real axis (see in Fig. 7), and accordingly C has to be opened up to C'. Thus, we obtain

$$\mathcal{G}(s,t_B)=\frac{1}{\pi}\int_{4m^2}^{\infty}ds'\frac{1}{s'-s}\left[\frac{1}{k(s')}\int_{t_-(s')}^{t_+(s')}(\Gamma)dt'\frac{1}{t_B-t'}\right]+2i\int_{s_-(t_B)}^{\infty}(C')ds'\frac{1}{s'-s}\frac{1}{U(s')},$$
$$\text{for } s<(M-m)^2. \tag{B6}$$

So, continuation in t is complete. Next, we need to continue s to the region $s\in[(M-m)^2,\infty]$; the continuation of first term on the right-hand side of Eq. (B6) shows no difficulty and encounters no extra singularities. However, as we can see in Fig. 4, s on the real axis is divided by contour C' into three sections, and thus, for $s\in[(M-m)^2,(M+m)^2]$, a pole contribution, $-4\pi/U(s)$, is picked up by the second term on the right-hand side of Eq. (B6). In the end, analytic continuation of the dispersion representation of $\mathcal{G}$ is given by

$$\mathcal{G}(s,t)=\frac{1}{\pi}\int_{4m^2}^{\infty}ds'\frac{1}{s'-s}\left[\frac{1}{k(s')}\int_{t_-(s')}^{t_+(s')}(\Gamma)dt'\frac{1}{t-t'}\right]+2i\theta(t)\theta(4m^2-t)\left[\int_{s_-(t)}^{s_+(\infty)}(C')ds'\frac{1}{s'-s}\frac{1}{U(s')}+\theta(s-(M-m)^2)\theta((M+m)^2-s)\frac{2\pi i}{U(s)}\right],$$
$$\text{for } (s,t)\in[-\infty,\infty]. \tag{B7}$$

2. Analytic continuation of the Pasquier inversion representation of the triangle diagram

For the analytic continuation of Eq. (B3), similarly, we start from region $t\in[4m^2,\infty]$, $s\in[-\infty,(M-m)^2]$. We first write Eq. (B3) as, see Eqs. (A7) and (A8),

$$\mathcal{G}(s,t)=\frac{1}{\pi}\int_{\Gamma'}\frac{dt'}{t-t'}\int_{s_{\Gamma'}(t)}^{\infty}(C')ds'\frac{1}{s'-s}\frac{1}{U(s')},$$
$$\text{for } t>4m^2,\qquad s<(M-m)^2. \tag{B8}$$

By exchanging the order of two integrals, we obtain

$$\mathcal{G}(s,t) = \frac{1}{\pi}\int_{C'} ds' \frac{1}{s'-s}\frac{1}{U(s')}\int_0^{t_{C'}(s')}(\Gamma')\frac{dt'}{t-t'},$$
$$\text{for } t > 4m^2, \qquad s < (M-m)^2. \tag{B9}$$

As we can see in Eq. (B9) and as also described previously in Sec. III, the s plane is divided by contour C'. Only for the region $s \in [(M-m)^2, (M+m)^2]$ does $\mathcal{G}$ need to pick up an extra term $2i/U(s)\int_0^{t_C(s)}(\Gamma)dt'/(t-t')$ to stay on the physical sheet, and thus the analytic continuation in s leads to

$$\mathcal{G}(s,t) = \frac{1}{\pi}\int_{-\infty}^{(M-m)^2}\frac{dt'}{t-t'}[\theta(t')\Delta(s,t') - \theta(-t')\Sigma(s,t')]$$
$$+\theta(s-(M-m)^2)\theta((M+m)^2-s)\frac{2i}{U(s)}\int_0^{t_C(s)}(\Gamma)\frac{dt'}{t-t'},$$
$$\text{for } t > 4m^2, \qquad s \in [-\infty,\infty]. \tag{B10}$$

Next, we continue t to below $4m^2$; again, the first term on the right-hand side of Eq. (B10) shows no difficulty of continuation and remains the same. From Fig. 9, we can see the t plane is divided by contour Γ, and thus only the second term on the right-hand side of Eq. (B10) for $t \in [0, 4m^2]$ needs to pick up a pole contribution, $-4\pi/U(s)$, to stay on the physical sheet. In the end, analytic continuation of the Pasquier inversion representation of $\mathcal{G}$ is given by

$$\mathcal{G}(s,t) = \frac{1}{\pi}\int_{-\infty}^{(M-m)^2}\frac{dt'}{t-t'}[\theta(t')\Delta(s,t') - \theta(-t')\Sigma(s,t')]$$
$$+2i\theta(s-(M-m)^2)\theta((M+m)^2-s)$$
$$\times\left[\frac{1}{U(s)}\int_0^{t_+(s)}(\Gamma)\frac{dt'}{t-t'} + \theta(t)\theta(4m^2-t)\frac{2\pi i}{U(s)}\right],$$
$$\text{for } (s,t) \in [-\infty,\infty]. \tag{B11}$$

[1] L. D. Faddeev, Zh. Eksp. Teor. Fiz. **39**, 1459 (1960) [Sov. Phys. JETP **12**, 1014 (1961)].
[2] L. D. Faddeev, *Mathematical Aspects of the Three-Body Problem in the Quantum Scattering Theory* (Israel Program for Scientific Translation, Jerusalem, Israel, 1965).
[3] J. G. Taylor, Phys. Rev. **150**, 1321 (1966).
[4] J.-L. Basdevant and R. E. Kreps, Phys. Rev. **141**, 1398 (1966).
[5] F. Gross, Phys. Rev. C **26**, 2226 (1982).
[6] N. N. Khuri and S. B. Treiman, Phys. Rev. **119**, 1115 (1960).
[7] J. B. Bronzan and C. Kacser, Phys. Rev. **132**, 2703 (1963).
[8] J. Gasser and H. Leutwyler, Nucl. Phys. **B250**, 539 (1985).
[9] J. Kambor, C. Wiesendanger, and D. Wyler, Nucl. Phys. **B465**, 215 (1996).
[10] A. V. Anisovich and H. Leutwyler, Phys. Lett. B **375**, 335 (1996).
[11] J. Bijnens and J. Gasser, Phys. Scr. **T99**, 34 (2002).
[12] J. Bijnens and K. Ghorbani, J. High Energy Phys. 11 (2007) 030.
[13] G. Colangelo, S. Lanz, and E. Passemar, *Proc. Sci.*, CD2009 (2009) 047.
[14] G. Colangelo, S. Lanz, H. Leutwyler, and E. Passemar, *Proc. Sci.*, EPS-HEP2011 (2011) 304.
[15] M. Zdrahal, K. Kampf, M. Knecht, and J. Novotny, *Proc. Sci.*, CD2009 (2009) 122.
[16] S. P. Schneider, B. Kubis, and C. Ditsche, J. High Energy Phys. 1102 (2011) 028.
[17] S. Lanz, *Proc. Sci.*, CD122013 (2013) 007.
[18] Y. Goradia and T. A. Lasinski, Phys. Rev. D **15**, 220 (1977).
[19] G. Ascoli and H. W. Wyld, Phys. Rev. D **12**, 43 (1975).
[20] I. J. R. Aitchison, II Nuovo Cimento **35**, 434 (1965).
[21] I. J. R. Aitchison, Phys. Rev. **137**, B1070 (1965); **154**, 1622 (1967).
[22] I. J. R. Aitchison and R. Pasquier, Phys. Rev. **152**, 1274 (1966).
[23] R. Pasquier and J. Y. Pasquier, Phys. Rev. **170**, 1294 (1968).
[24] R. Pasquier and J. Y. Pasquier, Phys. Rev. **177**, 2482 (1969).
[25] P. Guo, I. V. Danilkin, and A. P. Szczepaniak, arXiv: 1409.8652.
[26] F. Niecknig, B. Kubis, and S. P. Schneider, Eur. Phys. J. C **72**, 2014 (2012).
[27] I. V. Danilkin, C. Fernández-Ramírez, P. Guo, V. Mathieu, D. Schott, M. Shi, and A. P. Szczepaniak, arXiv:1409.7708.
[28] M. Hoferichter, B. Kubis, and D. Sakkas, Phys. Rev. D **86**, 116009 (2012).
[29] G. Colangelo, E. Passemar, and P. Stoffer, EPJ Web Conf. **37**, 05006 (2012).
[30] G. Colangelo, E. Passemar, and P. Stoffer, arXiv: 1501.05627.
[31] X.-W. Kang, B. Kubis, C. Hanhart, and Ulf-G. Meißner, Phys. Rev. D **89**, 053015 (2014).
[32] I. J. R. Aitchison and J. J. Brehm, Phys. Rev. D **17**, 3072 (1978).
[33] P. Guo, R. Mitchell, and A. P. Szczepaniak, Phys. Rev. D **82**, 094002 (2010).
[34] P. Guo, R. Mitchell, M. Shepherd, and A. P. Szczepaniak, Phys. Rev. D **85**, 056003 (2012).
[35] J. B. Bronzan, Phys. Rev. **134**, B687 (1964).
[36] G. F. Chew and S. Mandelstam, Phys. Rev. **119**, 467 (1960).
[37] G. Frye and R. L. Warnock, Phys. Rev. **130**, 478 (1963).
[38] I. J. R. Aitchison and C. Kacser, Phys. Rev. **133**, B1239 (1964).
[39] C. Kacser, J. Math. Phys. (N.Y.) **7**, 2008 (1966).
[40] I. J. R. Aitchison and C. Kacser, II Nuovo Cimento A **40**, 576 (1965).